Multistability in a neuron model with extracellular potassium dynamics

Xing-Xing Wu and J. W. Shuai*

Department of Physics and Institute of Theoretical Physics and Astrophysics, Xiamen University, Xiamen 361005, People's Republic of China

(Received 27 January 2012; revised manuscript received 24 April 2012; published 13 June 2012)

Experiments show a primary role of extracellular potassium concentrations in neuronal hyperexcitability and in the generation of epileptiform bursting and depolarization blocks without synaptic mechanisms. We adopt a physiologically relevant hippocampal CA1 neuron model in a zero-calcium condition to better understand the function of extracellular potassium in neuronal seizurelike activities. The model neuron is surrounded by interstitial space in which potassium ions are able to accumulate. Potassium currents, Na^+-K^+ pumps, glial buffering, and ion diffusion are regulatory mechanisms of extracellular potassium. We also consider a reduced model with a fixed potassium concentration. The bifurcation structure and spiking frequency of the two models are studied. We show that, besides hyperexcitability and bursting pattern modulation, the potassium dynamics can induce not only bistability but also tristability of different firing patterns. Our results reveal the emergence of the complex behavior of multistability due to the dynamical $[K^+]_o$ modulation on neuronal activities.

DOI: 10.1103/PhysRevE.85.061911 PACS number(s): 87.19.ll, 87.19.xm, 02.30.Oz

I. INTRODUCTION

Intra- and extraneuronal ion concentrations are not always constant. They are closely related to the behavior of electrically excitable neurons and in turn affect neuronal activity. As the main intracellular cation, the alteration of potassium concentration is associated with abnormal functions in the human body. In some pathological states of the central nervous system, such as hypoxia-induced spreading depression, a considerable rise of extracellular potassium was observed [1]. It has also been proposed that potassium concentration plays a key role in diseases, including diabetes and arrhythmias [2–4].

In 1956, Frankenhaeuser and Hodgkin observed the potassium accumulation during neuronal firing in the interstitial space around a squid giant axon [5] and then a regenerative hypothesis was proposed that the increased interstitial potassium concentration ($[K^+]_o$) contributes to higher neuronal excitability and a firing rate which in turn could create a further rise in $[K^+]_o$ [6]. It was observed that hippocampal epileptic activity was induced by a direct application of a high-potassium solution [7]. A later study argued that $[K^+]_o$ is only an influential factor in the course of neuronal firing, but could not initiate seizure activity [8]. Recent experiments showed that epilepsy is connected with a reduction of the Na^+-K^+ pump [9] and impairment of the glial K^+ uptake [10]. More recently, extracellular potassium accumulation and its function have attracted increasing attention. The effects of extracellular potassium concentration on firing patterns of low-calcium epileptiform activity have been investigated *in vivo* [11,12]. It has been also shown that the elevation of extracellular potassium concentration could play an active role in the modulation of cortical oscillatory activities [12].

Since Hodgkin and Huxley presented the HH model in 1952 [13], numerous computer simulations on the electrical behaviors of nervous system were carried out. Although most of them ignored the elevation of extracellular potassium, there have been some simulations taking into account the participation of potassium in neuronal behaviors. The modeling studies pointed out the critical roles of potassium concentration in modulating neuron dynamics. Based on a single neuron model, it is shown that the changes of $[K^+]_o$ can modulate the frequency of bursting [14]. With a two-compartment cortical neuron model, bistability with hysteresis between tonic firing and bursting is observed for elevated $[K^+]_o$ [15]. Efficient control of $[K^+]_o$ is shown to be responsible for the normal stability of brain function [16]. Furthermore, the recurring seizurelike events in a single cell are subject to local ion concentrations including $[K^+]_o$ [17,18].

In network models with potassium diffusion, it is suggested that $[K^+]_o$ dynamics can raise cellular excitability and influence neuronal behaviors in different stages of seizure discharges and spreading depression [19]. The modeling simulation also indicates that the balanced level of extracellular K^+ is needed to achieve local persistent activity that is stable to perturbations [20]. Moreover, potassium lateral diffusion has been proposed to be responsible for establishing a periodic neuronal firing in a small network [21,22].

It has been revealed that incorporating dendrite compartments alone accounts for qualitatively different activities at different stimulus currents [23]. But in most of the above-mentioned models with local ion concentration dynamics, the dendritic morphology is ignored. Here we consider a more biologically realistic neuron model with a dendritic structure and discuss the different spiking patterns in responding to a stimulus current with $[K^+]_o$ as a dynamical variable. In detail, we study a multicompartment hippocampal CA1 neuron model in a zero-calcium condition to better understand the effects of $[K^+]_o$ on the modulation of seizurelike activities. The model was suggested to simulate the CA1 neuron's electrophysiology including singlet, doublet, and triplet firing patterns responding to different depolarizing dc currents [23]. The model neuron was then modified to incorporate interstitial space around the soma to discuss the role of $[K^+]_o$ in nonsynaptic epilepsy [21].

In this paper, with the model in which the interstitial potassium concentration $[K^+]_o$ is allowed to evolve dynamically [21], we discuss bifurcation diagrams of the membrane

*jianweishuai@xmu.edu.cn

potential and interstitial potassium concentration as a function of stimulus current. The dendritic neuron shows not only singlet, doublet, and triplet firing patterns, but also a complex round-shaped burst. Besides the bistability of tonic spikes and bursts, a more interesting observation is that the $[K^+]_o$ dynamics can generate tristability over certain ranges of the stimulus current. These different spiking patterns are discussed with a reduced model in which $[K^+]_o$ is a constant. Based on a two-dimensional bifurcation analysis of the reduced model, we show that the slow dynamics of the extracellular potassium concentration is responsible for the multistability and plays a crucial role for the selection of attractors in the dendritic neuron.

II. CELL MODEL

The CA1 pyramidal model consists of 16 compartments with ten compartments for apical dendrites, five compartments for basal dendrites, and one single compartment for soma [Fig. 1(a)] [23]. The extracellular solution of the model neuron is characterized by zero-calcium concentration and a constant sodium concentration of 140 mM. The local increase in intracellular sodium concentration $[Na^+]_i$ or interstitial potassium concentration $[K^+]_o$ leads to a lower sodium reversal potential or higher potassium reversal potential, altering cellular excitability. However, as suggested in Ref. [17], the transient changes in $[K^+]_o$ have a greater effect over neuronal behavior than the changes in $[Na^+]_i$ due to the relatively small extracellular space. Therefore, only the interstitial potassium accumulated around the cell body is incorporated in the model [21,22].

In order to discuss the change of extracellular potassium concentration, the extracellular space has separated into two parts: the outside bath and the interstitial space (or K^+ shell)

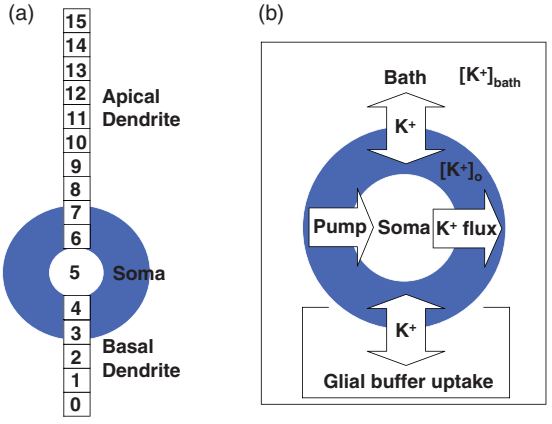

FIG. 1. (Color online) Structure of CA1 pyramidal cell model and schematic diagram of $[K^+]_o$-dependent mechanisms in the interstitial space around soma. (a) The 16-compartment CA1 pyramidal model includes ten compartments for the apical dendrites, five compartments for the basal dendrites, and a soma compartment surrounded by interstitial space. (b) During neuronal firing, three types of potassium ionic currents (I_{KDR}, I_{KA}, I_{KM}) result in K^+ accumulation in the interstitial space (blue/dark gray shell). Na^+-K^+ pumps and a glial buffer are introduced to regulate K^+ in the interstitial space. Potassium ions could also diffuse between the interstitial space and the bath where potassium concentration is considered constant.

immediately around the soma body [Fig. 1(b)]. In the bath solution the potassium concentration is assumed to be fixed at 8 mM, while in the interstitial space the potassium concentration $[K^+]_o$ is a variable, depicting the accumulation of potassium ions. Due to the fact that potassium ions accumulate more intensively in somatic layers than in dendritic layers [24], the K^+ shell is assumed to surround only the soma of the CA1 pyramidal neuron for simplicity [21].

In the model, the somatic compartment contains active ionic channels and only passive channels are included in dendrite compartments. There are five active ionic channels in the soma, i.e., a fast sodium current I_{Na}, a persistent sodium current I_{NaP}, and three potassium currents including a delayed rectifier current I_{KDR}, an A-type transient current I_{KA}, and a muscarinic current I_{KM}. The calcium and calcium-activated K^+ currents are not included under Ca^{2+}-free conditions. Then the dynamics of the membrane potential in the 16 compartments of the CA1 pyramidal model depends on the following ordinary differential equations:

$$C_s \frac{dV_s}{dt} = -(I_{Na} + I_{NaP} + I_{KDR} + I_{KA} + I_{KM} + I_{sLeak} + I_{pump}) + I_{sd} + I_{stim}, \quad (1)$$

$$C_d \frac{dV_{d,n}}{dt} = -I_{dLeak,n} + I_{dd,n} \quad (\text{where } n \neq 5,\ 0 \leqslant n \leqslant 15), \quad (2)$$

where V_s (soma) and $V_{d,n}$ (dendrites) are the transmembrane potential for the 16 compartments. I_{stim} is the injected electrical current applied to the somatic compartment. I_{sd} and I_{dd} are conductance currents between adjacent compartments. All these ionic and conductance currents for the soma and dendrites are described by the equations given in Table I.

The gating variables for the active ionic channels are m, h, w, n, a, b, and u. The corresponding dynamics is given by

$$\frac{dx}{dt} = \frac{x_\infty(V) - x}{\tau_x} = \alpha_x(V) - x(\alpha_x(V) + \beta_x(V)), \quad (3)$$

where $x : m,h,w,n,a,b$, and u. The detailed equations are given in Table II. Although theoretical problems could arise at certain values of V_s for several equations in Table II (i.e., both the numerator and denominator are zero), a numerical calculation almost never makes the membrane potential exactly equal to these values and so would not cause overflowing problems.

In the model neuron, by introducing a K^+ shell, the outside space of the soma is considered to consist of two parts: the interstitial space and the bath. The potassium concentration in the interstitial space can elevate from its resting value during spikes due to the K^+ release through potassium channels from the cytoplasm. The accumulated potassium ions could diffuse to the bath, while the Na^+-K^+ pump and glial buffer will react to high $[K^+]_o$ to remove excessive K^+ out of the interstitial space. Meanwhile, the continuously updated $[K^+]_o$ is always coupled with the membrane voltage via the Nernst equation. Those mechanisms that modulate potassium concentration in the interstitial shell surrounding the soma are depicted in Fig. 1(b). Thus, $[K^+]_o$ is a dynamical variable which is given by

$$\frac{d[K^+]_o}{dt} = J_{accumulation} + J^{diffusion}_{bath-shell} + J_{pump} + J^{uptake}_{glial-buffer}. \quad (4)$$

TABLE I. Currents and potassium flux.

Currents for dendrite compartments (μA/cm^2)
$I_{\mathrm{dLeak},n} = g_{\mathrm{dLeak}}(V_n - E_{\mathrm{L}})$
(where $n \neq 5; n \in [0,15]$)
$I_{\mathrm{dd},n} = g_{n-1,n}(V_{n-1} - V_n) + g_{n,n+1}(V_{n+1} - V_n)$
(where $n \neq 5; n \in [1,14]$)
$I_{\mathrm{dd},0} = g_{0,1}(V_1 - V_0)$
$I_{\mathrm{dd},15} = g_{14,15}(V_{14} - V_{15})$
Somatic currents (μA/cm^2)
$I_{\mathrm{Na}} = g_{\mathrm{Na}} m^3 h (V_{\mathrm{s}} - E_{\mathrm{Na}})$
$I_{\mathrm{NaP}} = g_{\mathrm{NaP}} w (V_{\mathrm{s}} - E_{\mathrm{Na}})$
$I_{\mathrm{KDR}} = g_{\mathrm{KDR}} n^4 (V_{\mathrm{s}} - E_{\mathrm{K}})$
$I_{\mathrm{KA}} = g_{\mathrm{KA}} ab (V_{\mathrm{s}} - E_{\mathrm{K}})$
$I_{\mathrm{KM}} = g_{\mathrm{KM}} u^2 (V_{\mathrm{s}} - E_{\mathrm{K}})$
where $E_{\mathrm{K}} = 26.71 \ln(\frac{[\mathrm{K}^+]_{\mathrm{o}}}{140})$mV
$I_{\mathrm{sLeak}} = g_{\mathrm{sLeak}}(V_{\mathrm{s}} - E_{\mathrm{L}})$
$I_{\mathrm{pump}} = I_{\mathrm{max}}/[1 + ([\mathrm{K}^+]_{\mathrm{eq}}/[\mathrm{K}^+]_{\mathrm{o}})]^2$
$I_{\mathrm{sd}} = g_{5,6}(V_6 - V_5) + g_{4,5}(V_4 - V_5)$
Somatic potassium concentration flux (mM/ms)
$J_{\mathrm{accumulation}} = \frac{(I_{\mathrm{KDR}} + I_{\mathrm{KA}} + I_{\mathrm{KM}}) \times \mathrm{A} \times 10^{-3}}{\mathrm{F} \times \mathrm{Volume}_{\mathrm{shell}}}$
$J_{\mathrm{pump}} = -\frac{2 \times I_{\mathrm{pump}} \times \mathrm{A} \times 10^{-3}}{\mathrm{F} \times \mathrm{Volume}_{\mathrm{shell}}}$
$J^{\mathrm{uptake}}_{\mathrm{glial\_buffer}} = r_{\mathrm{b}} \times ([\mathrm{B}]_{\mathrm{max}} - [\mathrm{B}]) - r_{\mathrm{f}} \times [\mathrm{K}^+]_{\mathrm{o}} \times [\mathrm{B}]$
where $r_{\mathrm{f}} = \frac{r_{\mathrm{f0}}}{1 + \exp[\frac{[\mathrm{K}^+]_{\mathrm{o}} - [\mathrm{K}^+]_{\mathrm{th}}}{-1.15}]}$
$J^{\mathrm{diffusion}}_{\mathrm{bath-shell}} = -\frac{([\mathrm{K}^+]_{\mathrm{o}} - [\mathrm{K}^+]_{\mathrm{bath}})}{\tau_{\mathrm{bs}}}$

The four K^+ fluxes are described by the equations given in Table I.

The buffering interactions between the interstitial potassium concentration $[K^+]_o$ and the concentration of the free buffer [B] is given by

$$\frac{d[\mathrm{B}]}{dt} = r_{\mathrm{b}} \times ([\mathrm{B}]_{\mathrm{max}} - [\mathrm{B}]) - r_{\mathrm{f}} \times [\mathrm{K}^+]_{\mathrm{o}} \times [\mathrm{B}], \qquad (5)$$

with binding and unbinding rates r_f and r_b, respectively. This equation has been used to describe buffering in the extracellular space [16].

The model parameters are shown in Table III. The area of the compartments has been taken into account to calculate the effective conductance and capacitance densities. All equations and parameters used for describing the CA1 neuron model come from Park *et al.* [21] with some necessary changes. For the reason that the Na^+-K^+ pump generates an electrogenic factor because it exchanges two K^+ ions for three Na^+ ions, it is thus reasonable that the potassium flux J_{pump} caused by the Na^+-K^+ pump should be twice as large as the flux suggested in Refs. [21,22] (see the corrected item for J_{pump} in Table I).

TABLE II. Kinetics for gating variables.

$\frac{dm}{dt} = \frac{11.7(11.5 - V_{\mathrm{s}})}{\exp(\frac{11.5 - V_{\mathrm{s}}}{13.7}) - 1.0}(1.0 - m) - \frac{0.4(V_{\mathrm{s}} - 10.5)}{\exp(\frac{V_{\mathrm{s}} - 10.5}{4.2}) - 1.0} m$
$\frac{dh}{dt} = \frac{0.67}{\exp(\frac{V_{\mathrm{s}} + 50.0}{5.5})}(1.0 - h) - \frac{2.24}{\exp(\frac{72.0 - V_{\mathrm{s}}}{29.0}) + 1.0} h$
$\frac{dw}{dt} = \frac{\frac{0.07}{\exp(\frac{-V_{\mathrm{s}} - 50.0}{2.0}) + 1.0} - w}{0.2}$
$\frac{dn}{dt} = \frac{0.00049 V_{\mathrm{s}}}{1.0 - \exp(\frac{-V_{\mathrm{s}}}{25.0})}(1.0 - n) - \frac{0.00008(V_{\mathrm{s}} - 10.0)}{\exp(\frac{V_{\mathrm{s}} - 10.0}{10.0}) - 1.0} n$
$\frac{da}{dt} = \frac{0.0224(V_{\mathrm{s}} + 30.0)}{1.0 - \exp(\frac{-V_{\mathrm{s}} - 30.0}{15.0})}(1.0 - a) - \frac{0.056(V_{\mathrm{s}} + 9.0)}{\exp(\frac{V_{\mathrm{s}} + 9.0}{8.0}) - 1.0} a$
$\frac{db}{dt} = \frac{0.0125}{\exp(\frac{V_{\mathrm{s}} + 8.0}{14.5})}(1.0 - b) - \frac{0.094}{\exp(\frac{-V_{\mathrm{s}} - 63.0}{16.0}) + 1.0} b$
$\frac{du}{dt} = 0.0084 \exp(\frac{V_{\mathrm{s}} + 26.0}{40.0})(1.0 - u) - \frac{0.0084}{\exp(\frac{V_{\mathrm{s}} + 26.0}{61.0})} u$

TABLE III. Parameter values.

R	Radius of cell	8.9×10^{-4} cm
A	Soma surface area	$4\pi R^2$
F	Faraday's constant	96485 C/mol
$[\mathrm{K}^+]_{\mathrm{bath}}$	Potassium concentration in the bath	8.0 mM
τ_{bs}	Diffusion time constant	800 ms
r_v	Ratio ($r_v = \mathrm{Volume}_{\mathrm{shell}}/\mathrm{Volume}_{\mathrm{cell}}$)	0.15
C_{s}	Soma capacitance	1.0 μF/cm^2
C_{d}	Dendrite capacitance	1.88 μF/cm^2
g_{Na}	Fast Na^+ conductance	20.0 mS/cm^2
g_{NaP}	Persistent Na^+ conductance	0.24 mS/cm^2
g_{KDR}	Delayed-rectifier K^+ conductance	22.0 mS/cm^2
g_{KA}	A-type transient K^+ conductance	3.0 mS/cm^2
g_{KM}	Muscarinic K^+ conductance	3.0 mS/cm^2
g_{sLeak}	Soma leakage conductance	1.8 mS/cm^2
$g_{4,5}, g_{5,6}$	Conductance between soma and dendrite	6.3 mS/cm^2
$g_{n,n+1}$	Conductance between dendrites	3.67 mS/cm^2
g_{dLeak}	Dendrite leakage conductance	0.0292 mS/cm^2
E_{Na}	Sodium reversal potential	65.0 mV
E_{L}	Leakage reversal potential	−46.0 mV
I_{max}	Pump maximal current	73.5 μA/cm^2
$[\mathrm{K}^+]_{\mathrm{eq}}$	Equilibrium potassium concentration	$[\mathrm{K}^+]_{\mathrm{bath}}$
$[\mathrm{B}]_{\mathrm{max}}$	Maximal buffer capacity	265 mM
r_{b}	Backward rate of buffer mechanism	0.0008/ms
r_{f0}	Forward rate of buffer mechanism	0.0008/mM/ms
$[\mathrm{K}^+]_{\mathrm{th}}$	Threshold $[\mathrm{K}^+]_{\mathrm{o}}$ for glial buffer	15 mM

In this paper we focus on the dynamic stable states of the neuron model responding to constant current. We found that to reach the stable state a transient period of 200 s is generally sufficient for the full model and 50 s for the reduced model. Most of our simulations were carried out using C++ with a Runge-Kutta fourth order algorithm and an integration time step of 0.005 ms. Bifurcation plots were also computed and confirmed by using XPPAUT [25] and OSCILL8 [26].

III. RESULTS

A. Analysis of the full model

We begin with a discussion of the system responding to different depolarizing dc currents I_{stim}. Figures 2(a)–2(c) show the effect of stimulus current I_{stim} on membrane potential V_s, spiking frequency f, and interstitial potassium concentration $[K^+]_o$ of the CA1 neuron model, respectively. To various intensities of the electrical stimuli, the model neuron responds differently with multistability in certain ranges. In order to plot Fig. 2, we first increase the values of I_{stim} from 0 to 80 μA/cm^2 with $\Delta I_{\mathrm{stim}} = 0.1$ μA/cm^2 and then decrease it back to 0. At each I_{stim}, the stable state is calculated after running the program for 200 s as a transient state. A set of values of the instantaneous stable state for the last I_{stim} is then used as the initial condition for the next I_{stim}. Then starting at $I_{\mathrm{stim}} = 11.2$ μA/cm^2 with a stable triplet state as

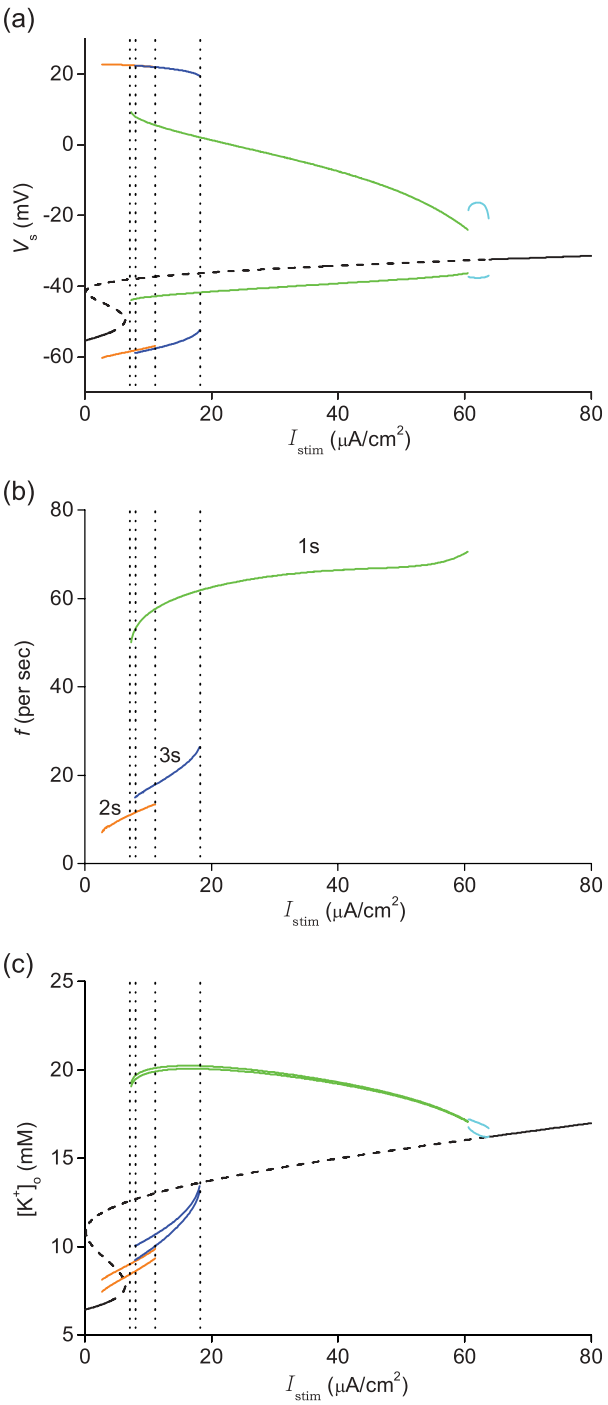

FIG. 2. (Color online) Bifurcation analysis of the full model with membrane potential (a) and interstitial potassium concentration (c) as a function of I_{stim}. (b) shows the oscillation frequency of the action potential. In each diagram (a), (c), the solid black line represents the stable steady states and the dashed black line represents the unstable steady states. The colored lines correspond to maximum and minimum values of periodic oscillatory states. A particular color denotes a certain type of neuronal firing pattern: green (gray) for a singlet spiking (1s), orange (medium gray) for doublet spiking (2s), and blue (dark gray) for triplet spiking (3s). Thus, three regions are defined by four vertical dotted lines, corresponding to multistability. For example, for the left region which is very narrow, the orange (medium gray) and green (gray) lines coexist, denoting the coexistence of singlet and doublet spiking.

the initial condition, we decrease I_{stim} to obtain the full range for triplet activity. The bifurcation plots were also computed and confirmed by using XPPAUT.

For small depolarizing stimuli below 3.8 μA/cm^2, the neuron is fixed at stable equilibrium states [shown as a black solid line in Figs. 2(a) and 2(c)]. At $I_{stim} \approx 3.8$ μA/cm^2, the stable equilibrium coalesces with a coexisting unstable equilibrium [dashed line in Figs. 2(a) and 2(c)] in a subcritical Hopf bifurcation. Then for $I_{stim} \in (3.8,63.9)$ μA/cm^2, oscillatory action potentials occur with oscillating $[K^+]_o$. This is depicted in Figs. 2(a) and 2(c) by lines that mark the maximum and minimum values of V_s and $[K^+]_o$. For increasing values of I_{stim} at $I_{stim} = 63.9$ μA/cm^2, the oscillating attractor eventually merges with the coexisting unstable equilibrium in another Hopf bifurcation. With $I_{stim} > 63.9$ μA/cm^2, the system becomes fixed again at stable equilibrium states, which are called depolarization blocks or spreadinglike depolarization [1,16,27].

In the oscillatory regime, the neuron system displays four qualitatively different firing patterns shown in Figs. 2(a) and 2(c) by different lines, including singlet spiking (1s, green/gray lines), doublet spiking (2s, orange/medium gray lines), triplet spiking (3s, blue/dark gray lines), and round-shaped bursting (cyan/light gray lines). Four examples are plotted in Fig. 3 with traces of somatic membrane potential V_s and interstitial potassium concentration $[K^+]_o$, including singlet [Fig. 3(a)], doublet [Fig. 3(b)], and triplet [Fig. 3(c)] activities, and round-shaped bursting [Fig. 3(d)]. Singlet mode activities (1s) correspond to the largest range of stimulus values [$I_{stim} \in (7.3,60.6)$ μA/cm^2] [Fig. 2(b)]. Doublet mode (2s) and triplet mode (3s) activities correspond to stimulus ranges for $I_{stim} \in (2.7,11.1)$ μA/cm^2 and $I_{stim} \in (7.9,18.1)$ μA/cm^2 [Fig. 2(b)], respectively. For these simple firing patterns, $[K^+]_o$ oscillates within a small range of concentration. The complex activities are found in a narrow range of stimulus values from 60.6 to 63.9 μA/cm^2. As plotted in Fig. 3(d), the system shows bursting activity with many spikes and an envelope of spiking amplitudes in each burst gives a round shape [Fig. 3(d)].

Figure 2(b) shows that the system's spiking frequency increases monotonically with an increase of I_{stim}. Although the spiking frequency keeps increasing, $[K^+]_o$ decreases with increasing I_{stim} at $I_{stim} > 15$ μA/cm^2 for singlet activity [Fig. 2(c)]. This happens due to the decreased action potential amplitude responding to the increasing I_{stim}, which plays a dominant role in modulating potassium concentrations at $I_{stim} > 15$ μA/cm^2. A decreased action potential amplitude and an almost constant interspike potential lead to smaller outward potassium currents. As a result, the increased firing frequency does not always correspond to increased $[K^+]_o$ for the singlet mode activity.

In this model neuron, the coupling between the excitable membrane voltage and slow extracellular potassium not only modulates the neuron's spiking patterns, but also gives rise to multistability between different spiking modes. Figure 2 shows three regions of multistability between two or three different spiking modes separated by vertical dotted lines. The system is bistable with singlet and doublet activities for a stimulus value ranging from 7.3 to 7.9 μA/cm^2. Another bistable regime where singlet and triplet activities coexist is observed at $I_{stim} \in (11.1,18.1)$ μA/cm^2. A more interesting observation is that,

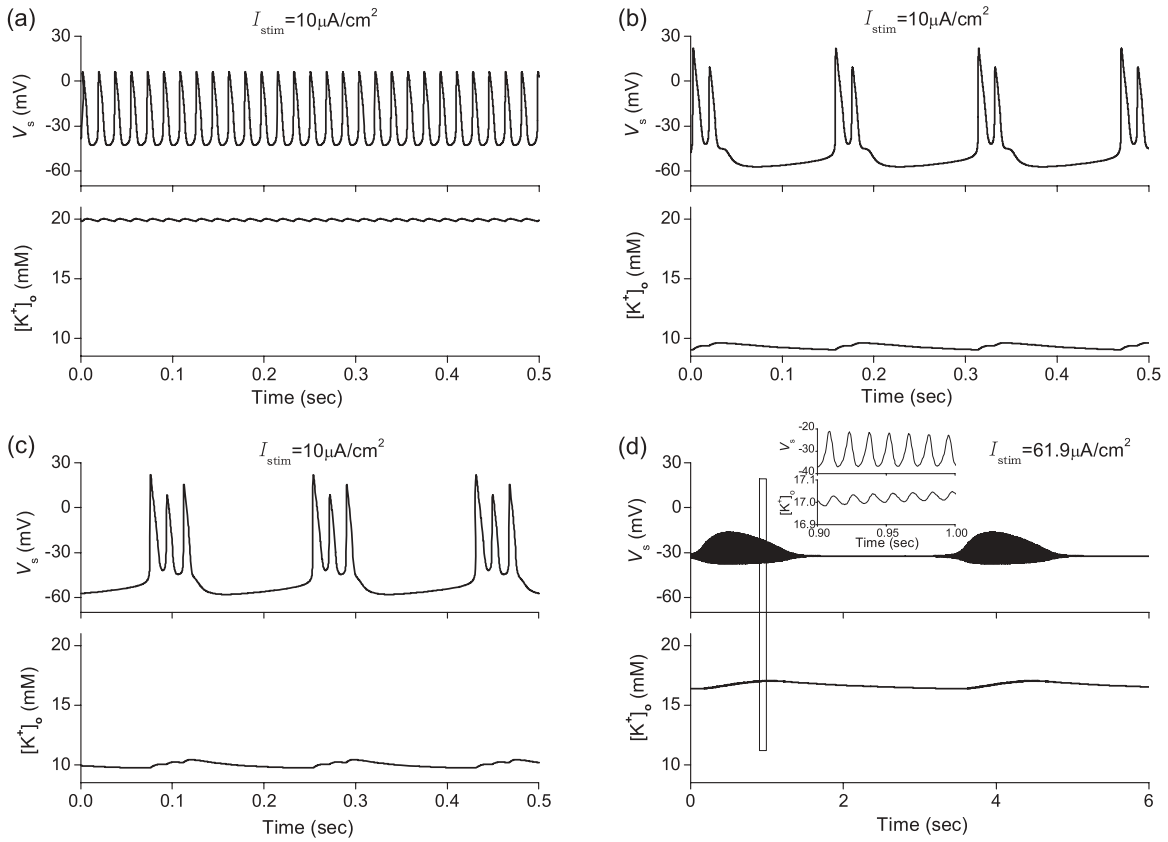

FIG. 3. The full model displays activities of singlet (a), doublet (b), and triplet modes (c), and round-shaped bursting mode (d). The upper and lower traces in each subfigure show the behavior of the action potentials and interstitial potassium oscillations, respectively. Responding to $I_{stim} = 10\ \mu A/cm^2$, three different spiking modes are observed, shown in (a)–(c) with the same voltage scale, the potassium scale, and the time scale. For (d), $I_{stim} = 61.9\ \mu A/cm^2$ with an inset of the enlargement of the rectangle part.

between these two bistability regions, i.e., the region at $I_{stim} \in (7.9,11.1)\ \mu A/cm^2$, tristability occurs where singlet, doublet, and triplet activities coexist. For example, responding to $I_{stim} = 10\ \mu A/cm^2$, three qualitatively different firing patterns are given in Figs. 3(a) and 3(b). One can also observe another common bistability between a steady state and an oscillatory state [$I_{stim} \in (2.7,3.8)\ \mu A/cm^2$]. Thus, our results show that coupling of a simple $[K^+]_o$ dynamics to the neuron system may lead to a rich behavior with multiple stability.

Here we show that $[K^+]_o$ is an important parameter to determine the selection of attractors in the region of multiple stability. As an example, we focus on the system at $I_{stim} = 10\ \mu A/cm^2$ where three attractors are observed. As shown in Figs. 2 and 3, the values of $[K^+]_o$ for these three attractors are in different ranges. In the simulation, we run the neuron program according to the model equations, but fix $[K^+]_o$ for 50 s at a constant value which is in the oscillating range of an attractor. After 50 s, we let $[K^+]_o$ also be freely updated according to the equations. Then after a transient period we check if the final attractor is still the attractor related to the initially fixed $[K^+]_o$. Hundreds of trials with different initial conditions show that the final attractors are typically the same ones related to the initially fixed $[K^+]_o$. This result indicates that $[K^+]_o$ is a crucial parameter for the selection of attractors.

Then we discuss the size of the attraction basins of $[K^+]_o$ of the various attractors. Because there are 25 variables in the system, it is difficult to discuss the attraction basin in detail. As a simple example, we only consider the instantaneous stable state when the somatic membrane is most polarized. We use such an instantaneous state as the initial condition but reset $[K^+]_o$ ranging from 2 to 35 mM. Then after a transient period we check which attractor the final stable state belongs to. Our simulation results for $I_{stim} = 10\ \mu A/cm^2$ are given as follows: For the singlet instantaneous state, the final attractor is still the singlet one if resetting $[K^+]_o > 14.3$ mM, while it becomes the triplet attractor if resetting $[K^+]_o < 14.3$ mM. For the doublet instantaneous state, the final attractor is still the doublet one if resetting $[K^+]_o < 14.9$ mM, while it becomes the triplet attractor if $[K^+]_o > 14.9$ mM. For the triplet instantaneous state, the final attractor is always the triplet one for any resetting $[K^+]_o$ from 2 to 35 mM. These results indicate that the triplet attractor has a large attraction basin of $[K^+]_o$ at $I_{stim} = 10\ \mu A/cm^2$.

B. Analysis of the reduced model

1. *One-dimensional bifurcation diagram*

We have shown how the neuron system responds to stimulus current with dynamical $[K^+]_o$. Different firing patterns and multistability are found in the model. The full model can be treated as a coupled model between a reduced neuron subsystem given by Eqs. (1)–(3) and the extracellular potassium

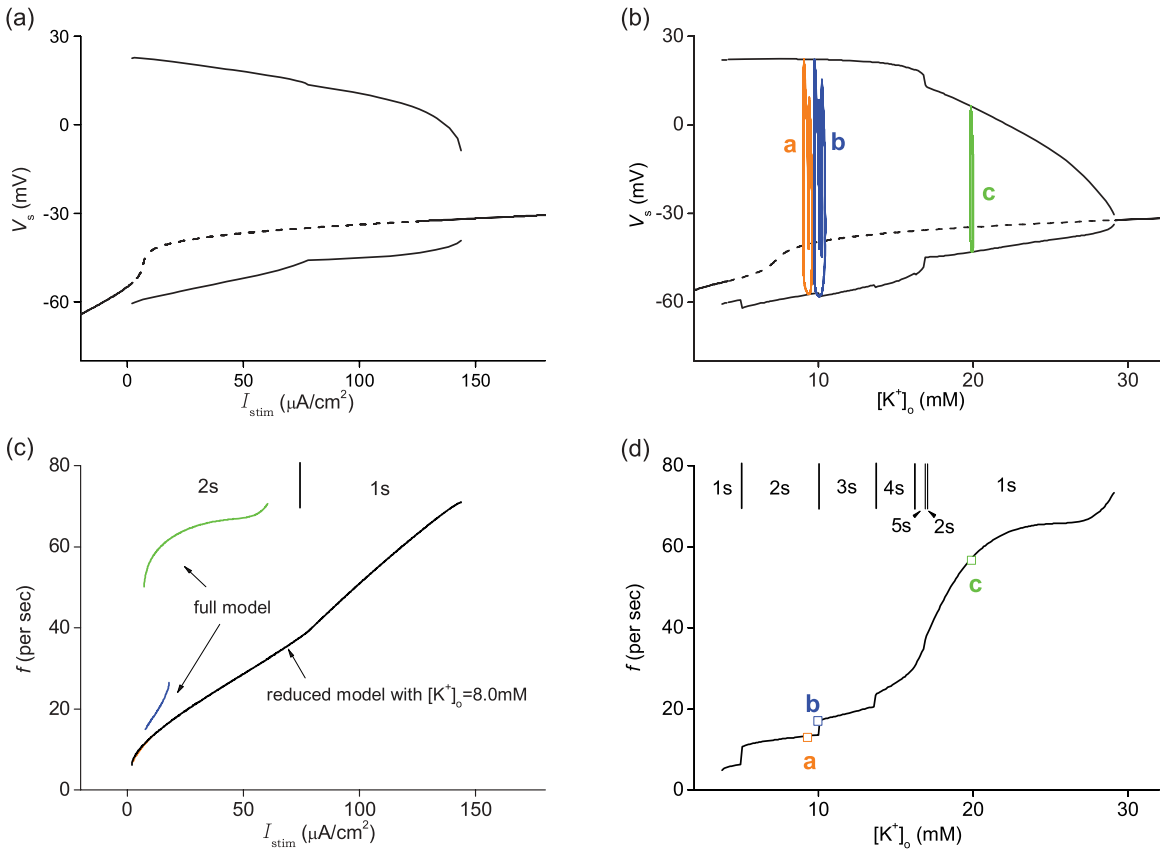

FIG. 4. (Color online) Bifurcation analysis of the reduced model with membrane potential as a function of I_{stim} at $[K^+]_o = 8$mM (a), or as a function of $[K^+]_o$ at $I_{stim} = 10\mu A/cm^2$ (b). Solid black lines represent stable states, while dashed black lines denote unstable fixed points. Periodic oscillatory behaviors are shown with maximum and minimum values. Spiking frequency, denoted by continuous black lines (c) and (d), corresponds to (a) and (b), respectively. Besides, spiking frequency curves of the full model shown in Fig. 2(b) are replotted in (c) with colored lines. Orange (medium gray), blue (dark gray), and green (gray) curves in (b) and open squares in (d) correspond to three spiking patterns in Figs. 3(a)–3(c).

subsystem given by Eqs. (4) and (5). The reduced neuron model is a fast subsystem, driving the extracellular potassium dynamics. As a feedback, the change of extracellular potassium concentration modulates the neuronal activity. To explore the mechanism of $[K^+]_o$ modulation in neuron behavior, we consider the reduced model given by Eqs. (1)–(3) by setting $[K^+]_o$ at fixed values and discuss its dynamics.

Figure 4(a) shows the bifurcation diagram of the membrane potential V_s as a function of I_{stim} by holding $[K^+]_o$ fixed at a resting concentration of 8 mM. The black solid line in Fig. 4(c) describes the spiking frequency as a function of I_{stim}, corresponding to the oscillatory region of Fig. 4(a). One can see that with I_{stim} very small or very large the reduced model shows the steady state, and in between the periodic firing patterns are observed, giving two modes only, singlet and doublet firing, while for the full model with dynamically variable $[K^+]_o$, four different firing patterns are observed (Fig. 3). Thus the modulation of $[K^+]_o$ enriches the neuronal spiking activities.

For comparison, the curves of spiking frequency via stimulus are plotted for the reduced model (black curve) and the full model (colored curves) in Fig. 4(c). The two models show different frequency curves. It is shown that in the oscillating region the spiking frequency of the full model is typically larger than the reduced model. This is because the current stimulus in the full model depolarizes the neuron and then the extracellular potassium accumulation during the neuronal firing causes the neuron to be further depolarized. Thus, $[K^+]_o$ and neuron depolarization feed on each other. As a result, the full model typically shows a larger firing frequency than that of the reduced model with a resting concentration $[K^+]_o = 8$ mM, when both models are stimulated persistently by a dc current with a particular intensity.

Now we discuss the dynamics of the reduced model responding to different $[K^+]_o$. Figures 4(b) and 4(d) show a bifurcation diagram of V_s and firing frequency f as a function of $[K^+]_o$ at $I_{stim} = 10\ \mu A/cm^2$. It can be seen that periodic firings are found for 3.8 mM $< [K^+]_o <$ 29.1 mM, in which the spiking frequency increases with an increase of $[K^+]_o$ and the neuron activity mode changes in order from singlet, to multiple-spike bursts (from 2-spike to 5-spike bursts), and finally to singlet.

For the full model, although $[K^+]_o$ is a dynamical variable, the change of $[K^+]_o$ is typically limited in a narrow range [Fig. 2(c)]. Thus the small oscillation of $[K^+]_o$ in the full model can be actually approximated by the reduced model with an averaged and so fixed $[K^+]_o$. In order to clarify this argument, we discuss a specific example at $I_{stim} = 10\ \mu A/cm^2$. The trajectory of membrane potential oscillations and $[K^+]_o$ for the

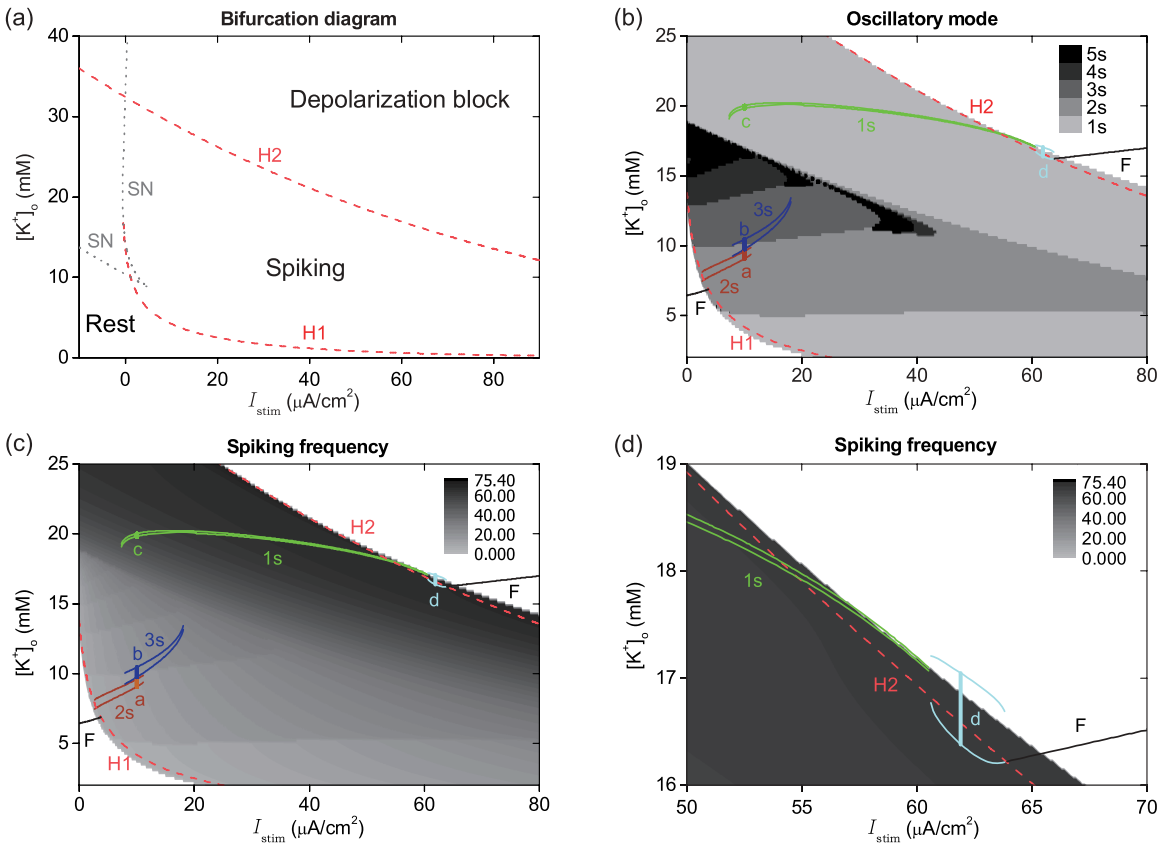

FIG. 5. (Color online) Two-dimensional bifurcation diagram of the reduced model with I_{stim} and $[K^+]_o$ as control parameters (a). The dotted and dashed lines denoted by SN (saddle-node bifurcation), H1 or H2 (Hopf bifurcation) divide the I_{stim}-$[K^+]_o$ space into several regions, including rest, spiking, and depolarization block regions. In the spiking region, the spiking mode (b) and the corresponding oscillation frequency (c) are represented by gray degrees. Near the Hopf bifurcation curves, the dashed lines separate narrow regions of oscillatory behavior in which a steady state coexists. (d) is an enlargement of (c) to show the region where round-shaped bursts (cyan/light gray lines) are observed in the full model. The bifurcation diagram, i.e., the maximum and minimum of $[K^+]_o$, via I_{stim}, of the full model [i.e., Fig. 2(c)] is also replotted in (b)–(d). Thus the black, green (gray), orange (medium gray), blue (dark gray), and cyan (light gray) lines are for fixed point (F), singlet ($1s$), doublet ($2s$), triplet ($3s$) spiking, and round-shaped burst of the full model, respectively. The oscillating ranges of $[K^+]_o$ of the four examples given in Fig. 3 are also plotted in (b)–(d) with short vertical lines a, b, c, and d.

full model shown in Figs. 3(a)–3(c) is projected on Fig. 4(b) with orange (medium gray), blue (dark gray), and green (gray) loops, representing doublet, triplet, and singlet modes, respectively. We see that the dynamical evolution of $[K^+]_o$ is slow enough to allow the projected trajectory to exactly follow the attracting periodic orbit predicted by the bifurcation diagram of the reduced model. Thus the firing activities given in Figs. 3(a)–3(c) for the full model with $I_{stim} = 10\ \mu A/cm^2$ can accordingly be discussed by the reduced model with constant $[K^+]_o = 9.3$, 10.1, and 19.9 mM, respectively. By this means, the corresponding firing frequencies calculated from the full model are plotted by open squares with orange (medium gray), blue (dark gray), and green (gray) colors in Fig. 4(d). One can see that these frequencies of the full model can be predicted by the reduced model accordingly.

2. *Two-dimensional bifurcation diagram*

Now we discuss the reduced model responding to the variation of both I_{stim} and $[K^+]_o$. A two-dimensional bifurcation diagram of the reduced model in I_{stim}-$[K^+]_o$ space is shown in Fig. 5(a). One can see that the Hopf (H1, H2) and saddle-node (SN) bifurcation curves are displayed as gray dotted and red dashed lines, respectively. In the region at the lower left of the Hopf bifurcation (H1) and saddle-node bifurcation (SN) curves, the reduced model mainly shows a resting steady state. The steady state of the depolarization block is observed above the Hopf bifurcation curve (H2). Between the resting and depolarization block states, the reduced model exhibits spiking activity.

The reduced model shows different spiking modes with different oscillation frequencies in the spiking region responding to different I_{stim} and $[K^+]_o$. As shown in Fig. 5(b), besides the singlet mode activity, the bursts with multispikes, as high as 5-spikes, are found in the reduced model. As plotted in Fig. 5(c) with a gray degree, the oscillation frequency in the spiking region increases with an increase of I_{stim} and $[K^+]_o$. One could clearly observe that not all of the gray points are inside the spiking region defined in Fig. 5(a). These narrow regions beyond the Hopf bifurcation curves show bistability

between a silent and spiking state of the reduced model. Thus the reduced model cell may also oscillate in some parts of rest and depolarization block regions.

Here we show that the dynamics of the full model (Fig. 2) can be understood based on the bifurcation diagram of the reduced model (Fig. 5). The bifurcation diagram of $[K^+]_o$ via I_{stim} for the full model [Fig. 2(c)] is overlapped in Figs. 5(b)–5(d). The two branches of the steady states (F, black lines in Fig. 5) for the full model are found in the regions of rest and depolarization block of the reduced model. If the values of $[K^+]_o$ of the full model responding to a certain I_{stim} are within the spiking region of the reduced model, an oscillating dynamics is typically observed for the full model.

For the full model, once a current stimulus I_{stim} is given, the possible values of $[K^+]_o$ are then determined. Because the dynamical ranges of $[K^+]_o$ for the full model are typically located in the regions of the $1s$, $2s$, and $3s$ modes of the reduced model [Fig. 5(b)], thus we mainly observed in the full model the spiking activities of singlet ($1s$, green/gray lines), doublet ($2s$, orange/medium gray lines), and triplet ($3s$, blue/dark gray lines). However, the 4-spike bursts or bursts with more spikes observed in the reduced model are not found in the full model. Because $[K^+]_o$ oscillates within a small range for the full model, its oscillating frequency can be approached by the spiking frequency of the reduced model at an averaged $[K^+]_o$ [Fig. 5(c)]. As a result, for the full model, the oscillations with $2s$, $3s$, and $1s$ modes have spiking frequency ranges of $7.1 < f < 13.4$, $15 < f < 26.5$, and $50.1 < f < 70.6$.

As for round-shaped bursts there is another scenario, which is shown in Fig. 5(d) with cyan (light gray) lines. We can see that the values of $[K^+]_o$ during the round-shaped burst for the full model traverse the Hopf bifurcation curve H2 of the reduced model. In detail, the maximum and minimum values of $[K^+]_o$ for the full model are located in the depolarization block region and the spiking region of the reduced model, respectively [cyan/light gray lines in Fig. 5(d)]. Thus, driven by I_{stim}, the slow variable $[K^+]_o$ oscillates between the spiking region and the steady state region determined by the reduced model. As a result, the full model shows a dynamics of repetitive transition between the fixed points and oscillatory spiking, leading to a round-shaped burst.

The bistability of a fixed point and an oscillatory state can be observed near the Hopf bifurcation points [Figs. 4(a), 4(b), and 5] in the reduced model. However, the reduced model does not show any coexistence of multiple spiking modes. Thus it is the dynamical $[K^+]_o$ that generates the multistability in the full model. The existence of the multistability between oscillatory attractors in the full model is based on different potassium levels. The potassium concentration dynamics is given by a competition between fast potassium currents and slow currents of sodium-potassium pumps, glia buffering, and extracellular potassium diffusion. In particular, corresponding to $I_{stim} = 10\ \mu A/cm^2$, the full model gains stability at three limit cycles with different potassium oscillations. The oscillating ranges of $[K^+]_o$ of these three patterns are also plotted in Figs. 5(b) and 5(c) with vertical lines a, b, and c. Different oscillating modes and firing frequencies in the full model are then determined by different dynamical locations in the reduced model.

IV. DISCUSSION

It is widely known that, persistently stimulated by an electrical stimulus, a neuronal activity will cause an increase of interstitial potassium concentrations, in turn further depolarizing the membrane. An increase in $[K^+]_o$ generates a larger firing rate or even brings out a depolarization block. In this paper, we showed that a single neuron model with both dynamical interstitial potassium concentrations and two dendritic branches exhibits four kinds of periodic firing behaviors, including singlet, doublet, and triplet spikes, and round-shaped bursts.

The full model is actually a coupled system between a membrane neuronal subsystem which is dynamically fast and the extracellular potassium subsystem which is dynamically slow. In order to clarify how $[K^+]_o$ dynamically modulates the neuronal activity, we furthermore considered a reduced model by freezing the extracellular potassium concentration at a constant value. Our simulations showed that different spiking activities are found in the full model with kinetic $[K^+]_o$ as a dynamical variable and the reduced model with constant $[K^+]_o$ as a control parameter. Only for the full model did we observe multistability of spiking modes and a round-shaped burst, while the 4-spike and 5-spike bursts are only found in the reduced model.

Nevertheless, we suggest that, due to the oscillating range of dynamical $[K^+]_o$ being rather small, the dynamics of the full model can be typically understood based on the discussion of the reduced model. Based on the two-dimensional bifurcation diagram of the reduced model on the plane of I_{stim} and $[K^+]_o$, we showed that singlet, doublet, or triplet spiking in the full model can be traced back to the reduced model with $[K^+]_o$ fixed at different values, while the complex round-shaped bursting mode in the full model can be explained by the reduced model with $[K^+]_o$ traversing slowly between a fixed point and a spiking orbit. Similar round-shaped bursts were also observed in experiments first [27,28] and then reproduced in neuronal simulations [17,18,29]

The multistability of different spiking activities was also observed in the model. The potassium-mediated bistability between tonic firing and bursting activities has been described in a cortical neuron with a burst generation due to the transition between two fixed points [15] and in a model of a leech heart interneuron due to the transition between a fixed point and a periodic orbit of the fast subsystem [30]. In this paper, a dynamics of potassium-induced multistability was discussed. Our full model showed the coexistence of several spiking or bursting activities when $[K^+]_o$ is a dynamical variable, while the reduced neuron model with constant $[K^+]_o$ showed no coexistence of multiple spiking modes. Thus, the bi- and tristability between several firing modes in the full model are a result of $[K^+]_o$ as a dynamical variable. We reported on the tristability induced by potassium dynamics in neuronal activity.

In conclusion, our results show the following: (1) The multistability, especially the tristability, with stable oscillatory activities has been observed in a single neuron over certain ranges of the stimulus current, (2) the dynamical nature of the potassium concentration is responsible for this multistability, and (3) the spiking pattern depends on the

final average potassium concentration achieved by competition between fast potassium currents and slow currents of sodium-potassium pumps, glia buffering, and extracellular potassium diffusion.

Simplification has been made in constructing the neuronal model. The realistic gradient distribution of the extracellular potassium concentration is simply digitized into binary values with $[K^+]_o$ in the interstitial space immediately around the soma body as a variable. A more accurate method to simulate the diffusion dynamics of extracellular potassium should be considered in future models. We assume that microenvironmental factors except for interstitial potassium do not modulate the neuronal response. For example, intracellular sodium accumulation could be considered to more accurately model the dynamics of the system. The increase in $[Na^+]_i$ will lead to a lower sodium reversal potential, which drives less sodium ions into the cell and consequently reduces neuronal excitability. A more realistic model may provide deeper insight on the effects of extracellular or intracellular ions on neuronal activity.

ACKNOWLEDGMENTS

The authors sincerely thank Dr. E.-H. Park for valuable discussions. Dr. D. P. Yang helped greatly in using OSCILL8 and in understanding the bifurcation analysis. J. W. Shuai acknowledges support from the National Science Foundation of China under Grant No. 30970970 and the China National Funds for Distinguished Young Scientists under Grant No. 11125419. Computational support from the Key Laboratory for Chemical Biology of Fujian Province, Xiamen University is gratefully acknowledged.

[1] M. Muller and G. G. Somjen, J. Neurophysiol. **83**, 735 (2000).
[2] E. I. Ekinci, K. Y. Cheong, M. Dobson, E. Premaratne, S. Finch, R. J. MacIsaac, and G. Jerums, Diabet. Med. **27**, 1401 (2010).
[3] L. M. Resnick, M. Barbagallo, L. J. Dominguez, J. M. Veniero, J. P. Nicholson, and R. K. Gupta, Hypertension **38**, 709 (2001).
[4] A. Zaza, Europace **11**, 421 (2009).
[5] B. Frankenhaeuser and A. L. Hodgkin, J. Physiol. **131**, 341 (1956).
[6] A. P. Fertziger and J. B. Ranck, Exp. Neurol. **26**, 571 (1970).
[7] E. C. Zuckermann and G. H. Glaser, Exp. Neurol. **20**, 87 (1968).
[8] U. Heinemann, H. D. Lux, and M. J. Gutnick, Exp. Brain Res. **27**, 237 (1977).
[9] W. R. Anderson, J. E. Franck, W. L. Stahl, and A. A. Maki, Epilepsy Res. **17**, 221 (1994).
[10] S. Gabriel, A. Eilers, A. Kivi, R. Kovacs, K. Schulze, T.-N. Lehmann, and U. Heinemann, Neurosci. Lett. **242**, 9 (1998).
[11] Z. Feng and D. M. Durand, Epilepsia **47**, 727 (2006).
[12] F. Amzica, M. Massimini, and A. Manfridi, J. Neurosci. **22**, 1042 (2002).
[13] A. L. Hodgkin and A. F. Huxley, J. Physiol. **117**, 500 (1952).
[14] M. Bazhenov, I. Timofeev, M. Steriade, and T. J. Sejnowski, J. Neurophysiol. **92**, 1116 (2004).
[15] F. Fröhlich and M. Bazhenov, Phys. Rev. E **74**, 031922 (2006).
[16] H. Kager, W. J. Wadman, and G. G. Somjen, J. Neurophysiol. **84**, 495 (2000).
[17] J. R. Cressman, G. Ullah, J. Ziburkus, S. J. Schiff, and E. Barreto, J. Comput. Neurosci. **26**, 159 (2009).
[18] E. Barreto and J. R. Cressman, J. Biol. Phys. **37**, 361 (2011).
[19] G. Florence, M. A. Dahlem, A. C. G. Almeida, J. W. M. Bassani, and J. Kurths, J. Theor. Biol. **258**, 219 (2009).
[20] G. Ullah, J. R. Cressman, E. Barreto, and S. J. Schiff, J. Comput. Neurosci. **26**, 171 (2009).
[21] E. H. Park and D. M. Durand, J. Theor. Biol. **238**, 666 (2006).
[22] E. H. Park, Z. Feng, and D. M. Durand, Biophys. J. **95**, 1126 (2008).
[23] J. Shuai, M. Bikson, P. J. Hahn, J. Lian, and D. M. Durand, Biophys. J. **84**, 2099 (2003).
[24] G. G. Somjen and J. L. Giacchino, J. Neurophysiol. **53**, 1098 (1985).
[25] [http://www.math.pitt.edu/∼bard/xpp/xpp.html].
[26] [http://sourceforge.net/projects/oscill8/].
[27] M. Bikson, P. J. Hahn, J. E. Fox, and J. G. R. Jefferys, J. Neurophysiol. **90**, 2402 (2003).
[28] J. Ziburkus, J. R. Cressman, E. Barreto, and S. J. Schiff, J. Neurophysiol. **95**, 3948 (2006).
[29] G. Ullah and S. J. Schiff, PLoS Comput. Biol. **6**, e1000776 (2010).
[30] A. Shilnikov, R. L. Calabrese, and G. Cymbalyuk, Phys. Rev. E **71**, 056214 (2005).